for Scientific Research on Innovative Areas (S.T.), Grants-in-Aid for Young Scientists (B) (K.T.), and Platform for Drug Discovery, Information, and Structural Life Science from the Ministry of Education, Culture, Sports, Science and Technology of Japan; and the Japan New Energy and Industrial Technology Development Organization (NEDO) and the National Institute of Biomedical Innovation (Y.F.). H.S., Y.Y., and A.T. screened claudin genes; H.S. performed protein expression, purification, and electron microscopic studies; T.N. crystallized the mCldn15 protein in lipidic cubic phase, collected and processed diffraction data, and solved and refined the structure; K.T. analyzed the structure; R.I. assisted with x-ray data collection and structure determination; N.D. performed mass spectrometric analyses; H.S., T.N., K.T., S.T., O.N., and Y.F. wrote the manuscript; and S.T., O.N., and Y.F. supervised the research. The authors declare no competing financial interests. Coordinates and structure factors have been deposited in the Protein Data Bank under accession number 4P79.

Supplementary Materials
www.sciencemag.org/content/344/6181/304/suppl/DC1
Materials and Methods
Table S1
Figs. S1 to S11
References (*30*–*47*)

15 November 2013; accepted 26 March 2014
10.1126/science.1248571

The Structural Basis of Pathogenic Subgenomic Flavivirus RNA (sfRNA) Production

Erich G. Chapman,[1,2] David A. Costantino,[1,2] Jennifer L. Rabe,[1] Stephanie L. Moon,[3] Jeffrey Wilusz,[3] Jay C. Nix,[4] Jeffrey S. Kieft[1,2]*

Flaviviruses are emerging human pathogens and worldwide health threats. During infection, pathogenic subgenomic flaviviral RNAs (sfRNAs) are produced by resisting degradation by the 5′→3′ host cell exonuclease Xrn1 through an unknown RNA structure-based mechanism. Here, we present the crystal structure of a complete Xrn1-resistant flaviviral RNA, which contains interwoven pseudoknots within a compact structure that depends on highly conserved nucleotides. The RNA's three-dimensional topology creates a ringlike conformation, with the 5′ end of the resistant structure passing through the ring from one side of the fold to the other. Disruption of this structure prevents formation of sfRNA during flaviviral infection. Thus, sfRNA formation results from an RNA fold that interacts directly with Xrn1, presenting the enzyme with a structure that confounds its helicase activity.

Flaviviruses (FVs, including Dengue, West Nile, Yellow Fever, Japanese Encephalitis, and others) are single-stranded positive-sense RNA viruses and emerging worldwide human health threats (*1*–*3*). During infection by arthropod-borne FVs, not only is the viral genomic RNA (gRNA) replicated, but specific 300- to 500-nucleotide-long subgenomic flaviviral RNAs (sfRNAs) also accumulate (*4*–*9*). These sfRNAs relate directly to disease, being essential for FV pathogenicity in fetal mice and for cytopathicity in cultured cells (*5*), through several proposed mechanisms (*10*–*13*). sfRNAs are produced through incomplete degradation of viral gRNA by the 5′→3′ host-cell exonuclease Xrn1 (*14*), which halts at defined locations within the gRNA's 3′ untranslated region (3′UTR), forming sfRNAs (fig. S1A) (*5*). Biochemical studies suggest that independently folded RNA structures are responsible for this programmed Xrn1 resistance (*15*–*17*); however, the structure-based mechanism remains unknown.

Xrn1 resistance is conferred by discrete RNA sequences conserved across FVs that we refer to as Xrn1-resistant RNAs (xrRNAs) (*15*). Alignment of putative xrRNA sequences (fig. S1B) suggests a shared structure that includes a three-way junction surrounded by conserved nucleotides and the potential to form a pseudoknot (Fig. 1A) (*5*, *16*, *17*). To identify xrRNAs suitable for structural studies, we used a previously validated assay using purified Xrn1 from *Kluyveromyces lactis* to test the Xrn1 resistance of putative xrRNAs from different arthropod-borne FVs (*15*); all were resistant in vitro (fig. S1C). The sequence alignments and functional data suggest that the structure of any one FV xrRNA is representative of all; therefore, we determined the structure of a functional xrRNA from Murray Valley Encephalitis (MVE) Virus (Fig. 1, B and C) to 2.5 Å resolution using x-ray crystallography (fig. S2). The RNA adopts a compact structure with helices P1 and P2 stacked coaxially and helix P3 at an acute angle relative to P1 (Fig. 1D), which is consistent with other RNA three-way junctions of this class (fig. S3) (*18*). Helices P1 and P3 form a ringlike structure defined by nucleotides 33 to 49, which comprise a continuous loop that resides entirely on one side of the structure. The 5′ end of the xrRNA passes directly through the center of the ring, crossing from one side of the structure to the other (fig. S4). The ringlike side of the xrRNA that Xrn1 encounters as it approaches in a 5′→3′ direction (the "front") is concave, with the phosphate backbone defining the rim of the concavity, the major groove as the inner surface, and the RNA that the enzyme must pull into the active site emerging from the center (Fig. 1D). In the crystal structure, the putative RNA pseudoknot is not formed, but the relevant bases are in a conformation where they can readily pair; this would allow the P4-L*4* hairpin to stack under helix P3. The structure shows that the pseudoknot is not essential for folding of the three-way junction, formation of the ring, or placement of the 5′ end through the ring; however, it does enhance resistance (fig S5, A and B). Stem-loop P4-L4 does not interact with the rest of the xrRNA and can be removed without compromising Xrn1 resistance (fig. S5C) (*15*). Upon encountering the xrRNA, Xrn1 must pull the 5′ end of the RNA through the ring. Rather than simply unwinding a prototypical RNA helix, unfolding this xrRNA requires that Xrn1 essentially turn the structure inside out (Fig. 2A). In contrast, the virally encoded RNA-dependent RNA polymerase approaching from the 3′ end during (–) strand synthesis would not encounter this impediment, suggesting that the three-dimensional topology confers the characteristic of unidirectional resistance.

The three-helix junction is the core of the xrRNA structure but is not independently folded; its structure depends on interactions with the 5′ end (Fig. 2B and fig S7, A to C). Specifically, C5 base-pairs with G46, and this pair stacks on a platform formed by intrastrand pairing of U47 with the Hoogsteen face of A49 (Fig. 2B). This stacking diverts the RNA chain to the space between P1 and P3, where U4 makes a base triple in the major groove of the A24-U38 pair; all three of these nucleotides are absolutely conserved. This interaction holds P1 and P3 together in a conformation further stabilized by inner-sphere coordination of a magnesium ion by the phosphates of C5 and A6 (fig. S7D). The next-most 5′ nucleotide, G3, forms a Watson-Crick (WC) base pair with junction nucleotide C40. Disruption of this base pair by mutation of either base (G3C and C40G) abolished the ability of the MVE RNA to resist Xrn1 degradation (Fig. 2C). The double mutant (G3C+C40G), designed to restore the base pairing, did not restore resistance. This is likely due to the formation of incorrect but stable structure induced by mutation, precluding restoration of proper base-pairing interactions in the double mutant (the C40G mutant could form a C-G pair with C22 that G3C cannot compete with). An additional intramolecular interaction involves U2, which was mutated to a G in the crystallized RNA. Nucleotide A41 in the three-way junction is poised to form a Watson-Crick pair with U2 in the wild-type (WT) sequence, and there is covariation between these positions (fig. S1, B and D). Together, this suggests the U2-A41 pair naturally forms; however, the structure folds

[1]Department of Biochemistry and Molecular Genetics, School of Medicine, University of Colorado Denver, Aurora, CO 80045, USA. [2]Howard Hughes Medical Institute, School of Medicine, University of Colorado Denver, Aurora, CO 80045, USA. [3]Department of Microbiology, Immunology and Pathology, Colorado State University, Fort Collins, CO 80523, USA. [4]Molecular Biology Consortium, Advanced Light Source, Lawrence Berkeley National Laboratory, Berkeley, CA 94720, USA.

*Corresponding author. E-mail: jeffrey.kieft@ucdenver.edu

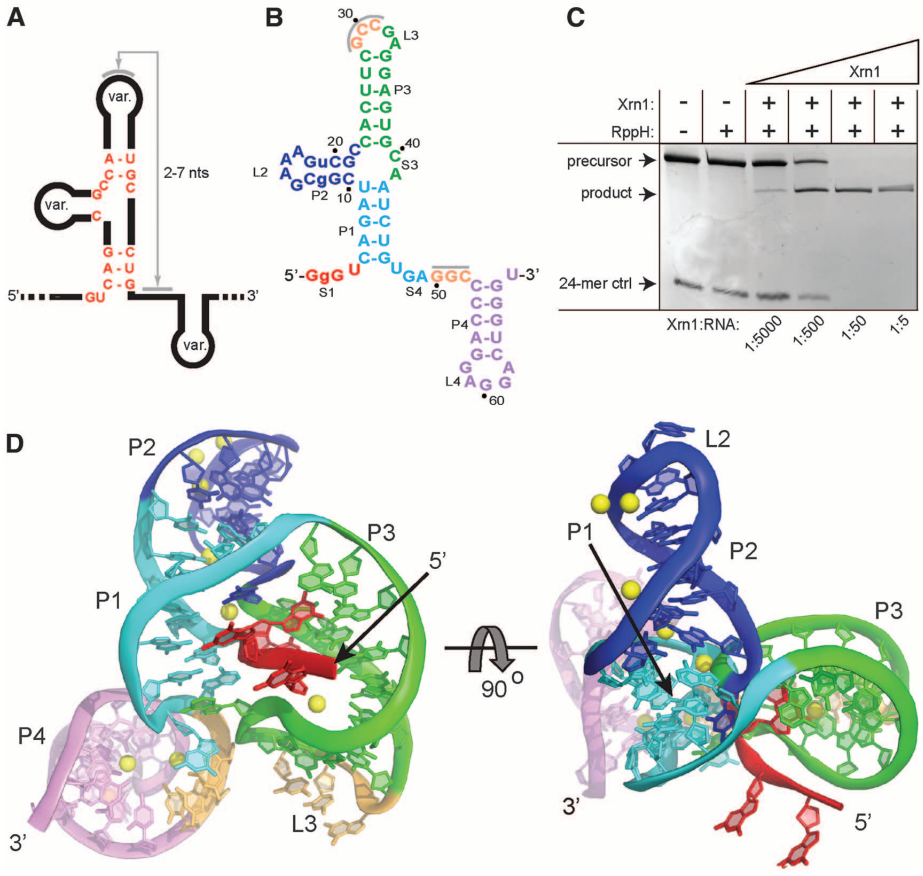

Fig. 1. Crystal structure of an xrRNA. (**A**) Conserved secondary structure and sequence (red) of xrRNAs. "Var." indicates elements of variable size and sequence. (**B**) Crystallized RNA sequence from MVE. Lower-case nucleotides were altered from wild type. The U2G mutation was made to increase transcription yields, but neither this nor the other mutation affected function (C). Gray bars indicate a putative pseudoknot interaction. (**C**) Gel demonstrating Xrn1 resistance by the crystallized RNA, using an assay with Xrn1 from *K. lactis* that was validated in a previous publication (*15*). The precursor is the crystallized RNA with a 30-nt 5′ leader. A 24-oligomer monophosphorylated RNA was included as a control for Xrn1 activity. Under these conditions, each Xrn1 molecule processes multiple copies of the xrRNA, and there is no in-trans protection of the 24-oligomer. This does not preclude a role for sfRNA as a transient Xrn1 inhibitor during infection (*11*, *15*). (**D**) Two views of the structure, colored to match (B). Yellow indicates Mg^{2+} ions.

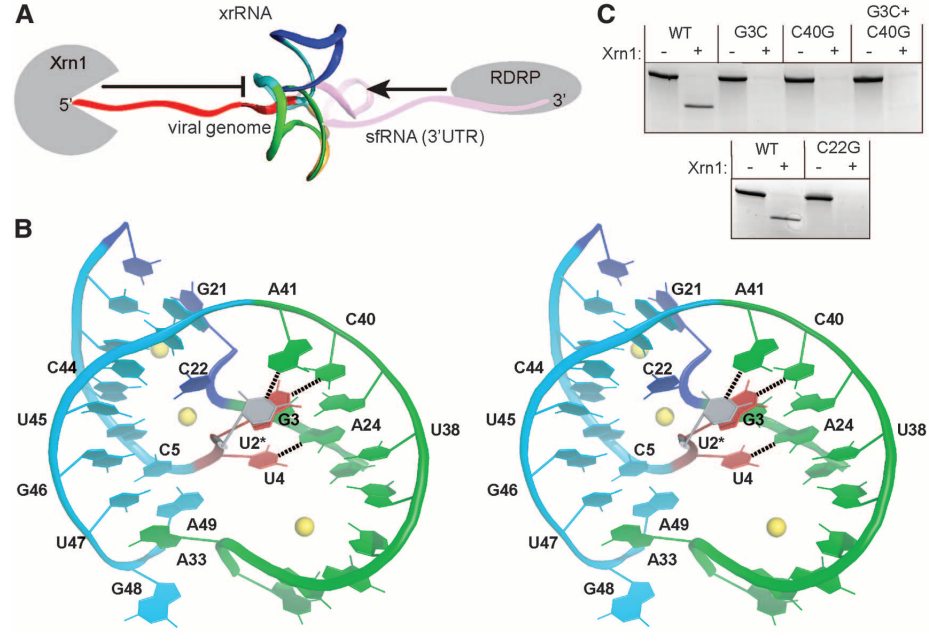

Fig. 2. Formation and importance of the junction and ring structures. (**A**) Structure (backbone ribbon) placed in context with upstream and downstream RNA and enzymes that approach from each side (not to scale). (**B**) Stereo view of the P1-P3 ring and 5′ end of the xrRNA, colored to match (A) and Fig. 1D. U2, which was mutated to a G, is shown modeled in position in gray. Base pairs between the 5′ nucleotides and P3 are shown with dashed lines. (**C**) Xrn1 resistance assays of mutant RNAs based on these interactions (mutant sequences are provided in fig. S6A).

and resists Xrn1 even when it is not present. The only nucleotide in the three-way junction that does not make base pair interactions with the 5′ end of the RNA is C22, which makes hydrogen bonds with U43, C44, and perhaps U45 through phosphates, nucleobase functional groups, and C22's 2′-hydroxyl (fig. S7E). Mutation of conserved C22 (C22G) eliminates Xrn1 resistance in vitro by the crystallized MVE RNA (Fig. 2C), by xrRNAs from Dengue, and from the Kunjin strain of West Nile Virus (WNV_{KUN}; a proven model for FV infection) and also disrupts sfRNA production during WNV_{KUN} infection (*15*).

The U2-A41 and G3-C40 base pairs comprise a second, previously unidentified pseudoknot in the xrRNA structure between S1 and S3 that is interwoven with the S4-L3 pseudoknot (fig. S8). Within the structure, these pseudoknot interactions couple the junction conformation with positioning of the 5′ end of the xrRNA through

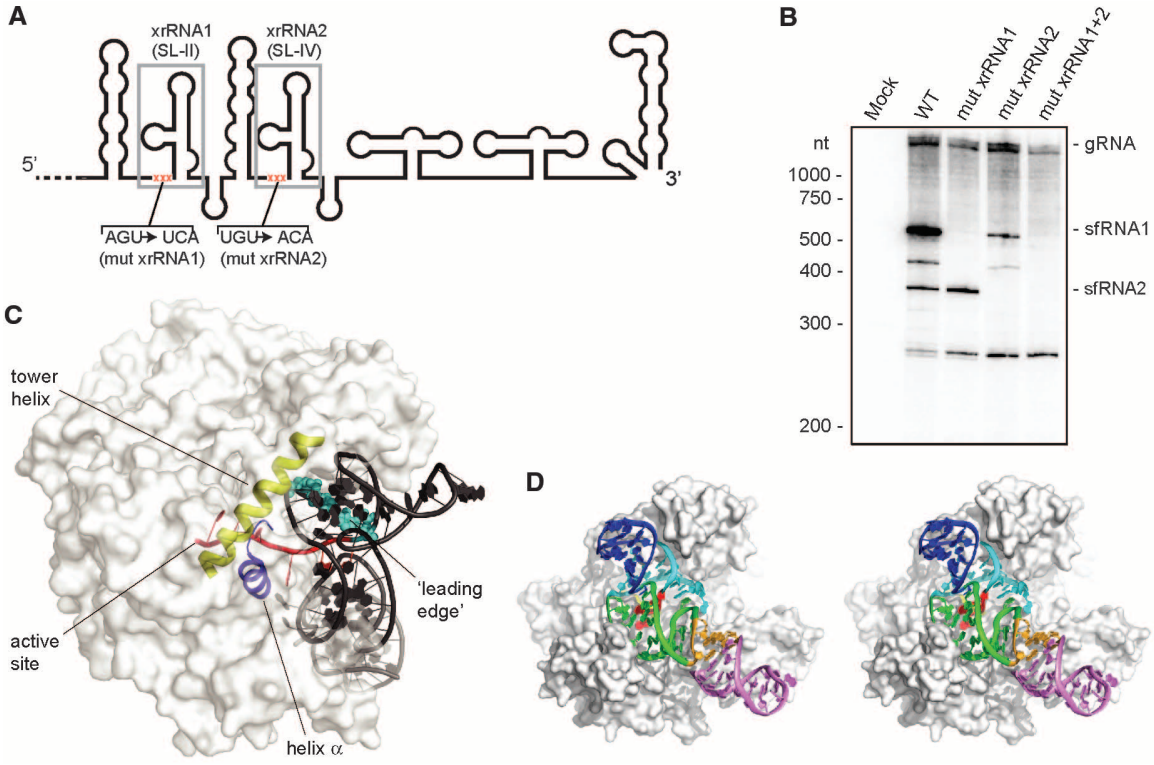

Fig. 3. Importance of the structure during infection and proposed mechanism of resistance. (**A**) Secondary structure cartoon of the 3′UTR from WNV_{KUN}. Two xrRNAs are boxed in gray, and the location of mutations is shown in red. (**B**) Northern blot analysis of total RNA isolated from human cells infected with the wild type and mutant WNV_{KUN} (mutant sequences are provided in fig. S6B). The location of molecular weight markers and the identity of sfRNA species are indicated to the left and right of the blot, respectively. (**C**) Model xrRNA structure on *D. melanogaster* Xrn1 (white surface) (fig. S9). The tower helix (yellow) and helix α (blue) involved in helicase activity, the active site, the RNA entering the active site (red), and leading edge of the helix to be unwound (light blue) are shown. (**D**) Stereo view of model showing how the xrRNA fits in a cleft in Xrn1's surface.

the P1/P3 ring. To test the importance of these structural features during infection, we disrupted the three 5′-most nucleotides in two xrRNA structures in WNV_{KUN} (Fig. 3A and fig. S6B) and monitored sfRNA production during infection in human cells by these viruses. WT virus produces multiple sfRNAs; the two largest, sfRNA1 and sfRNA2, are produced by Xrn resistance of xrRNA1 and xrRNA2, respectively (Fig. 3B). Mutation of xrRNA1 (mut xrRNA1) (fig. S6B) eliminated sfRNA1 production, mutation of xrRNA2 (mut xrRNA2) (fig. S6B) eliminated sfRNA2 production [mut xrRNA2 also decreased sfRNA1 production as has been reported previously (*15*)], and a double mutant (mut xrRNA1+2) (fig. S6B) eliminated both sfRNA1 and sfRNA2, indicating the 5′ end-junction interaction is essential for sfRNA formation during infection. The P1/P3 ring is closed on the side opposite the junction by extrusion and stacking of A33 on the U47-A49 platform at the base of P1 (Fig. 2B). Although folding of the 5′ end with the junction is sufficient to form the ring, we propose that closing of the S4-L3 pseudoknot provides the final "latch" that fully stabilizes the conformation (fig. S5A). Consistent with this, chemical probing suggests that the S4-L3 pseudoknot is conformationally dynamic or transiently formed and that the structure of the three-way junction, the 5′ end, and the pseudoknot are coupled (*15*).

We mapped the 5′ terminus of the RNA product resulting from resistance to a point 2 nucleotides upstream of the 5′ end of the RNA we crystallized (fig. S9A), which is consistent with studies of other xrRNAs (*4*, *5*, *15*, *17*). Using the structure of Xrn1 from *Drosophila melanogaster* bound to a substrate analog (*19*), we modeled the xrRNA structure in position with the last nucleotide to be processed in the Xrn1 active site (Fig. 3, C and D, and fig. S9, B to D). When the enzyme halts, the xrRNA directly contacts Xrn1's surface, positioned in a cleft, with its ring structure braced over the entry to the active site and conserved nucleotides in position to contact the protein (fig. S1D). The Xrn1-xrRNA contacts may further stabilize the xrRNA fold or prevent conformational changes hypothesized to be important for helicase activity. It is proposed that Xrn1's helicase activity is conferred by Brownian motion and the enzyme's "tower helix" and "helix α," which interact and unwind with the leading edge of an RNA duplex as it is pulled into the cleft over the active site (*19*). The model shows that the xrRNA structure is braced against the enzyme, holding the leading edge of the relevant RNA duplex behind the concave ring structure and away from these helices, suggesting a mechanism for RNA structure-driven Xrn1 resistance and, by extension, sfRNA production.

References and Notes

1. S. Bhatt *et al.*, *Nature* **496**, 504–507 (2013).
2. J. S. Mackenzie, D. J. Gubler, L. R. Petersen, *Nat. Med.* **10** (suppl.), S98–S109 (2004).
3. D. Normile, *Science* **342**, 415 (2013).
4. K. C. Lin, H. L. Chang, R. Y. Chang, *J. Virol.* **78**, 5133–5138 (2004).
5. G. P. Pijlman *et al.*, *Cell Host Microbe* **4**, 579–591 (2008).
6. G. Wengler, G. Wengler, H. J. Gross, *Virology* **89**, 423–437 (1978).
7. C. W. Naeve, D. W. Trent, *J. Virol.* **25**, 535–545 (1978).
8. H. Takeda, A. Oya, K. Hashimoto, T. Yasuda, M. A. Yamada, *J. Gen. Virol.* **38**, 281–291 (1978).
9. N. Urosevic, M. van Maanen, J. P. Mansfield, J. S. Mackenzie, G. R. Shellam, *J. Gen. Virol.* **78**, 23–29 (1997).
10. A. Schuessler *et al.*, *J. Virol.* **86**, 5708–5718 (2012).
11. S. L. Moon *et al.*, *RNA* **18**, 2029–2040 (2012).
12. E. Schnettler *et al.*, *J. Virol.* **86**, 13486–13500 (2012).
13. J. A. Roby, G. P. Pijlman, J. Wilusz, A. A. Khromykh, *Viruses* **6**, 404–427 (2014).
14. C. I. Jones, M. V. Zabolotskaya, S. F. Newbury, *Wiley Interdiscip. Rev. RNA* **3**, 455–468 (2012).
15. E. G. Chapman, S. L. Moon, J. Wilusz, J. S. Kieft, *eLife* (2014).
16. A. Funk *et al.*, *J. Virol.* **84**, 11407–11417 (2010).
17. P. A. Silva, C. F. Pereira, T. J. Dalebout, W. J. Spaan, P. J. Bredenbeek, *J. Virol.* **84**, 11395–11406 (2010).
18. A. Lescoute, E. Westhof, *RNA* **12**, 83–93 (2006).
19. M. Jinek, S. M. Coyle, J. A. Doudna, *Mol. Cell* **41**, 600–608 (2011).

Acknowledgments: We thank the members of the Kieft Lab for discussions and A. Ferré-d'Amaré, M. Johnston, and R. Batey for critical reading of this

manuscript. The University of Colorado Denver X-ray Facility is supported by University of Colorado Cancer Center Support Grant P30CA046934. J.S.K. is an Early Career Scientist of the Howard Hughes Medical Institute. J.W. was supported by a NIH award through the Rocky Mountain Regional Center of Excellence, U54 AI-065357. Coordinates and structure factors have been deposited with Protein Data Bank accession code 4PQV.

Supplementary Materials

www.sciencemag.org/content/344/6181/307/suppl/DC1
Materials and Methods
Figs. S1 to S9
Table S1
References

15 January 2014; accepted 24 March 2014
10.1126/science.1250897

The STAT3-Binding Long Noncoding RNA lnc-DC Controls Human Dendritic Cell Differentiation

Pin Wang,[1,2] Yiquan Xue,[1] Yanmei Han,[1] Li Lin,[2] Cong Wu,[3] Sheng Xu,[1] Zhengping Jiang,[1] Junfang Xu,[3] Qiuyan Liu,[1] Xuetao Cao[1,2,3]*

Long noncoding RNAs (lncRNAs) play important roles in diverse biological processes; however, few have been identified that regulate immune cell differentiation and function. Here, we identified lnc-DC, which was exclusively expressed in human conventional dendritic cells (DCs). Knockdown of lnc-DC impaired DC differentiation from human monocytes in vitro and from mouse bone marrow cells in vivo and reduced capacity of DCs to stimulate T cell activation. lnc-DC mediated these effects by activating the transcription factor STAT3 (signal transducer and activator of transcription 3). lnc-DC bound directly to STAT3 in the cytoplasm, which promoted STAT3 phosphorylation on tyrosine-705 by preventing STAT3 binding to and dephosphorylation by SHP1. Our work identifies a lncRNA that regulates DC differentiation and also broadens the known mechanisms of lncRNA action.

The mammalian genome transcribes numerous long noncoding RNAs (lncRNAs), and only some of them have been functionally characterized (*1*). Although a number of lncRNA molecules have been reported to play crucial roles in diverse processes and diseases (*2*–*4*), only a few examples of lncRNAs that regulate the immune system have been described (*5*–*7*).

Dendritic cells (DCs) are the most potent antigen-presenting cells in mammalian immune systems; their differentiation and function influences the outcome of innate and adaptive immune response (*8*). Although several transcription factors (*9*, *10*) and cytokines (*11*) have been identified as playing critical roles in the generation and homeostasis of DC populations, whether noncoding RNA, especially lncRNAs, play a role in DC differentiation and function is largely unknown.

Unlike the well-established mechanism of microRNA action, which is based on seed sequence base-pairing (*12*, *13*), lncRNAs' mode of action remains to be fully understood (*14*). A few lncRNAs exert their functions through interacting with heteronuclear proteins or chromatin modification complexes in the nucleus (*15*–*18*), whereas others are reported to affect mRNA stability or translation in the cytoplasm (*19*–*21*). Whether there are other unknown functional modes for lncRNAs is unclear.

To identify lncRNAs involved in DC differentiation and function, we utilized the well-accepted model of human DC differentiation from peripheral blood monocytes (*22*) and conducted transcriptome microarray analysis (Fig. 1A) and RNA sequencing (RNA-seq) (Fig. 1B). Both methods identified a modestly conserved intergenic lncRNA

[1]National Key Laboratory of Medical Immunology and Institute of Immunology, Second Military Medical University, Shanghai 200433, China. [2]National Key Laboratory of Molecular Biology and Department of Immunology, Institute of Basic Medical Sciences, Chinese Academy of Medical Sciences, Beijing 100005, China. [3]Institute of Immunology, Zhejiang University School of Medicine, Hangzhou 310058, China.

*Corresponding author. E-mail: caoxt@immunol.org

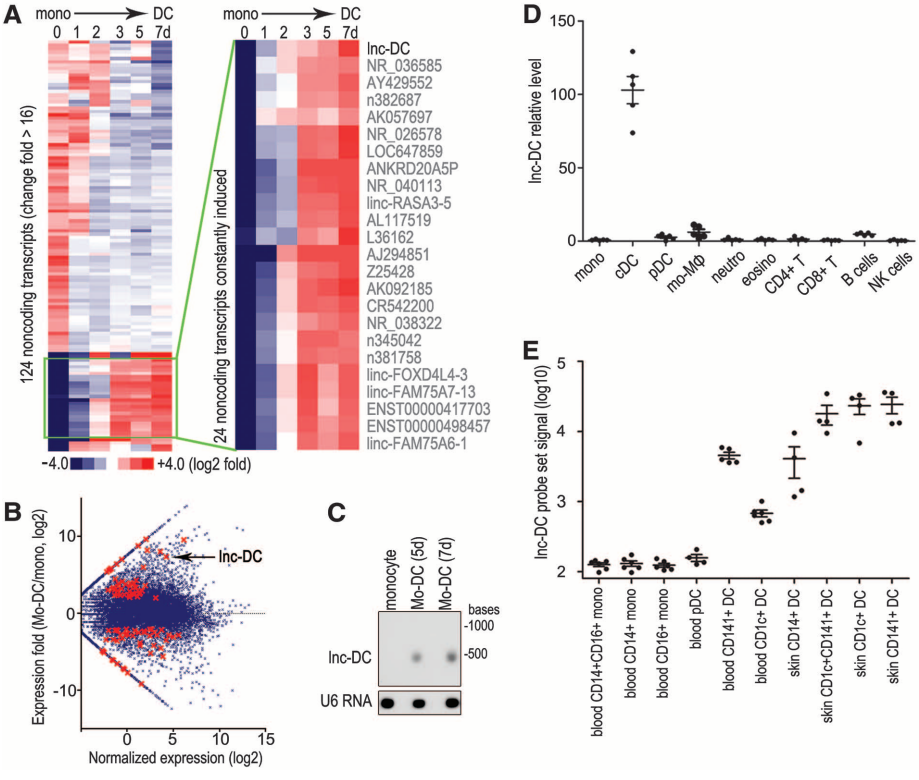

Fig. 1. lnc-DC is highly expressed in human cDC subsets. (A) The cluster heat map shows lncRNAs with expression change fold >16 from microarray data ($P < 0.05$). **(B)** Ratio of gene expression in Mo-DC to monocytes (vertical axis) and average expression of genes in Mo-DC versus that in monocytes (horizontal axis), presented as a Bland-Altman plot of our RNA-seq analysis. Highlighted in red are 99 lncRNAs with significant changes in expression (fold > 4, false discovery rate < 0.05). **(C)** Northern blotting of lnc-DC in monocytes and Mo-DC. U6 RNA serves as a loading control. Unless noted otherwise, all results in this and other figures were representative of at least three independent experiments. **(D)** qPCR detection of lnc-DC in immune cell subsets sorted from human peripheral blood. Data are normalized to glyceraldehyde-3-phosphate dehydrogenase (GAPDH) expression and monocytes (mono), which are set to a value of 1. NK cells, natural killer cells. **(E)** lnc-DC expression levels (signal intensity of probe set ILMN_3200140) in distinct DC/mono subsets of human blood and skin from GSE35457 data.